Turbulent Rayleigh-Bénard convection in strong vertical magnetic field

R. Akhmedagaev[1], O. Zikanov[1]†, D. Krasnov[2] and J. Schumacher[2]

[1]University of Michigan - Dearborn, 4901 Evergreen Road, Dearborn, MI 48128-1491, USA
[2]Technische Universität Ilmenau, Postfach 100565, Ilmenau, D-98694, Germany

(Received xx; revised xx; accepted xx)

Direct numerical simulations are carried out to study flow structure and transport properties in turbulent Rayleigh-Bénard convection in a cylindrical cell of aspect ratio one with an imposed axial magnetic field. Flows at the Prandtl number 0.025 and the Rayleigh and Hartmann numbers up to 10^9 and 1400 are considered. The results are consistent with those of earlier experimental and numerical data. As anticipated, the heat transfer rate and kinetic energy are suppressed by strong magnetic field. At the same time, their growth with the Rayleigh number is found to be faster in flows at high Hartmann numbers. This behaviour is attributed to the newly discovered flow regime characterized by prominent quasi two-dimensional structures reminiscent of vortex sheets observed earlier in simulations of magnetohydrodynamic turbulence. Rotating wall modes similar to those in the Rayleigh-Bénard convection with rotation are found in flows near the Chandrasekhar linear stability limit. Detailed analysis of the spatial structure of the flows and its effect of global transport properties is reported.

1. Introduction

Combined turbulent thermal convection and magnetic fields significantly affect flow structure and transport of momentum and heat in electrically conducting fluids. The effect plays an important role in numerous systems found in technology and nature (Ozoe 2005; Weiss & Proctor 2014; Davidson 2016). Prominent technological examples are the liquid metal batteries, growth of semiconductor crystals, and design of blankets and divertors in nuclear fusion reactors. The notable example of a natural system is the planetary dynamo. We consider the basic configuration of the Rayleigh-Bénard convection (RBC) in a cylinder with thermally insulating sidewalls and an imposed vertical magnetic field. The quasistatic approximation of low magnetic Reynolds $Re_m \ll 1$ and Prandtl $P_m \ll 1$ numbers typical for laboratory experiments and industrial processes with liquid metal flows is utilized to describe the electromagnetic interactions. This implies that the applied magnetic field $\boldsymbol{B}_0$ is much stronger than the induced one $\boldsymbol{b}$ (Davidson 2016). The induced magnetic field is neglected in the expressions for the Lorentz force and Ohm's law. Furthermore, the induced field is assumed to adjust instantaneously to changes of velocity. The flow-field interaction is, essentially, approximated as one-way influence of the magnetic field on the flow.

The effect of the vertical magnetic field on RBC has been studied experimentally (Nakagawa 1957; Cioni *et al.* 2000; Aurnou & Olson 2001; Burr & Müller 2001; King & Aurnou 2015; Zürner *et al.* 2020), numerically (Liu *et al.* 2018; Yan *et al.* 2019; Akhmedagaev *et al.* 2020) and theoretically (Chandrasekhar 1961; Houchens *et al.* 2002;

---

† Email address for correspondence: zikanov@umich.edu

Busse 2008). The dynamics of the system is determined by three dimensionless control parameters: the Rayleigh, Hartmann and Prandtl numbers

$$Ra = \frac{g\alpha \varDelta T H^3}{\nu\kappa}, \quad Ha = B_0 H\sqrt{\frac{\sigma}{\rho\nu}}, \quad Pr = \frac{\nu}{\kappa}, \tag{1.1}$$

with the acceleration due to gravity g, the thermal expansion coefficient α, the temperature difference between the horizontal boundaries of the fluid layer $\varDelta T$, the height of the layer H, the kinematic viscosity ν, the temperature diffusivity κ, the electrical conductivity σ, the mass density ρ and the magnetic permeability of free space μ_0. Systems with lateral walls add the aspect ratio $\varGamma = D/H$ as a parameter, where D is the typical horizontal size, the diameter of the cylinder in our case.

The classical picture of the effect of magnetic field on RBC in an infinite horizontal layer includes suppression of turbulence (Nakagawa 1957) and increase of the critical Rayleigh number Ra_c of the convection onset. The latter effect is given by Chandrasekhar (1961) in the asymptotic form at high Ha as $Ra_c \approx \pi^2 Ha^2$. The dominance of quasi-two-dimensional (Q2D) cellular and columnar structures in the flows at $Ra > Ra_c$ within a layer with stress-free boundary conditions was observed by Yan *et al.* (2019). These regimes are uniquely identified by the slope of the Nusselt $Nu(Ra)$ and Reynolds $Re(Ra)$ numbers, the physical structure of the flows, and the relative relative sizes of terms in the governing equations. The flow regimes are identified as Q2D when the velocity and temperature fields are virtually independent of the axial direction outside of the boundary layers near the top and bottom walls.

Theoretical analysis of Busse (2008) predicts that the presence of the sidewalls leads to onset of convection at much lower Ra than in an infinite layer. The heat transfer in that case is concentrated near the walls. Recent numerical simulations (Liu *et al.* 2018) of RBC in a rectangular cell at $Ra \sim Ra_c$ and $Ra < Ra_c$ confirmed existence of this so-called wall mode regime, in which significant flow and heat transfer are limited to narrow zones near the sidewalls (the wall modes). These modes are planar jets at moderate Ha, but have complex two-layer structure at high Hartmann numbers, higher than $Ha_c \equiv \sqrt{Ra}/\pi \approx 1000$. Wall modes are also found in simulations of RBC in a cylindrical cell at $\varGamma = 4$, $Pr = 0.025$, $Ha \leqslant 1000$, $Ra = 10^7$ (Akhmedagaev *et al.* 2020). The simulations results are consistent with the recent extensive measurements of RBC with vertical magnetic field in a cylinder with moderate Ra and Ha by Zürner *et al.* (2019, 2020).

We also should mention a certain similarity between the behaviour found in RBC with vertical magnetic field and that in convection with rotation around vertical axis. Formation of Q2D structures, faster growth of heat transfer rate with Ra at high rotation rates, and wall modes are observed in rotating systems (Zhong *et al.* 1991; Ecke *et al.* 1992; Zhang *et al.* 2019).

The focus of our investigation is on the RBC with vertical magnetic field and sidewalls at $Ra \gg Ra_c$. High-resolution DNS of flows in a cylindrical cavity with $\varGamma = 1$, $Pr = 0.025$, $10^7 \leqslant Ra \leqslant 10^9$ and $0 \leqslant Ha \leqslant 1400$ are performed. The work follows the experiments by Cioni *et al.* (2000) carried out at the same $\varGamma$ and Pr (mercury) and at $Ra \leqslant 3\times 10^9$, $Ha \leqslant 2000$ (the highest Ra and Ha achieved so far). The experiments have shown that the slope β of the asymptotic power law $Nu \backsim Ra^\beta$ increases from $\beta \approx 0.26$ in non-magnetic flows to up to $\beta \approx 1$ at high Ha. The result is that the heat transfer rate in high-Ra flows in very strong magnetic fields becomes comparable to the rate in turbulent flows without the magnetic field. The physical mechanisms determining this behaviour remain uncertain.

To the best of our knowledge, this study is the first to analyze turbulent RBC at high Ha and realistically low Pr in the framework of high resolution DNS. The only related simulations have been performed by Lim *et al.* (2019) in a cubic convection cell at unrealistic $Pr = 8$ with Ra up to 10^{10} and Ha up to 800.

2. Presentation of the problem

2.1. *Physical model*

We consider a flow of an incompressible, viscous, electrically conducting fluid (a liquid metal) with constant physical properties contained in a cylinder with a uniform axial magnetic field. The governing equations are made dimensionless by using the cylinder's height H, the free-fall velocity $U = \sqrt{g\alpha \Delta T H}$, the external magnetic field strength B_0 and the imposed temperature difference $\Delta T = T_{bottom} - T_{top}$ as the scales of length, velocity, magnetic field and temperature, correspondingly. The Boussinesq and quasi-static approximations are used. The equations are

$$\boldsymbol{\nabla} \cdot \boldsymbol{u} = 0, \tag{2.1}$$

$$\frac{\partial \boldsymbol{u}}{\partial t} + (\boldsymbol{u} \cdot \boldsymbol{\nabla})\boldsymbol{u} = -\boldsymbol{\nabla} p + \sqrt{\frac{Pr}{Ra}}(\boldsymbol{\nabla}^2 \boldsymbol{u} + Ha^2\,(\boldsymbol{j} \times \boldsymbol{e}_z)) + T\boldsymbol{e}_z, \tag{2.2}$$

$$\frac{\partial T}{\partial t} + \boldsymbol{u} \cdot \boldsymbol{\nabla} T = \sqrt{\frac{1}{Ra Pr}}\boldsymbol{\nabla}^2 T, \tag{2.3}$$

$$\boldsymbol{j} = -\boldsymbol{\nabla}\phi + (\boldsymbol{u} \times \boldsymbol{e}_z), \tag{2.4}$$

$$\boldsymbol{\nabla}^2 \phi = \boldsymbol{\nabla} \cdot (\boldsymbol{u} \times \boldsymbol{e}_z), \tag{2.5}$$

where p, $\boldsymbol{u}$, ϕ and T are the fields of pressure, velocity, electric potential, and deviation of temperature from a reference value. The top and bottom walls are maintained at constant temperatures $T = -0.5$ and $T = 0.5$, respectively. The lateral wall is thermally insulated, so having $\partial T/\partial n = 0$. No-slip boundary conditions for velocity are applied at the walls. All walls are perfectly electrically insulated which implies $\partial \phi/\partial n = 0$.

2.2. *Numerical method*

Governing equations (2.1) – (2.5) are solved numerically using the finite difference scheme described earlier by Krasnov *et al.* (2011, 2012); Zhao & Zikanov (2012); Zikanov *et al.* (2013). Performance of the method in applications to convection with magnetic field was analyzed in comparison with other methods, in particular with the finite-volume approach by Gelfgat & Zikanov (2018). The spatial discretization is implemented in the cylindrical coordinates with the boundary conditions at the axis specified as discussed by Zikanov *et al.* (2013). The scheme is of the second order and nearly fully conservative in regards of the mass, momentum, kinetic energy, and electric charge conservation principles (Krasnov *et al.* 2011; Ni *et al.* 2007). The time discretization is semi-implicit and based on the Adams-Bashforth/Backward-Differentiation method of the second order. Implicit treatment is applied to the diffusive term in (2.3) and the azimuthal derivative part of the Laplacian in (2.2). The radial and axial parts of the viscous term in (2.2) are treated explicitly. At every time step, three elliptic equations – the projection method equation for pressure, the equation for temperature and the potential equation (2.5) – are solved using the FFT in the azimuthal direction and the cyclic reduction solver in the $r - z -$ plane. The computational grid is clustered toward the walls according to the coordinate transformation in the axial direction $z = \tanh(A_z\zeta)/\tanh(A_z)$ and in the radial direction $r = 0.9\sin(\eta\pi/2) + 0.1\eta$. Here $-1 \leqslant \zeta \leqslant 1$, $0 \leqslant \eta \leqslant 1$ are the virtual uniform coordinates, in which the grid is uniform. The novel features that appear in the new version of the algorithm and its thorough verification are presented by Akhmedagaev *et al.* (2020).

2.3. *Numerical simulations*

All the results presented below are for the stage of a fully developed flow. The non-magnetic flows are taken as initial conditions for magnetoconvection flows. Global transport properties of momentum and heat transfer are quantified by the Reynolds number $Re = u_{rms}\sqrt{Ra/Pr}$ with $u_{rms} = \langle u_r^2 + u_z^2 + u_\theta^2 \rangle_{V,t}$ and the Nusselt number $Nu = 1 + \sqrt{RaPr}\langle u_z T \rangle_{V,t}$ where $\langle \cdot \rangle_{V,t}$ stands for volume and time averaging, correspondingly. The time averaging is performed over at least 100 convective time units.

2.4. *Grid sensitivity study*

The results of the grid sensitivity study are summarized in the supplementary materials. Verification of the model in comparison with experimental and numerical data is discussed in section 3.2. Here we briefly discuss the grid requirements and the grids used in our simulations. In addition to internal structure of the flow, four boundary layers need to be accurately resolved (Grossmann & Lohse 2001; Davidson 2016): the thermal boundary layer of thickness $\delta_T \approx 1/(2Nu)$, the viscous boundary layer with $\delta_v \approx 1/(4\sqrt{Re})$, the Shercliff layer with $\delta_{Sh} = 1/\sqrt{Ha}$ at the lateral wall, and the Hartmann layer with $\delta_{Ha} = 1/Ha$ at the top and bottom walls.

We find that grids with $N = N_r \times N_z \times N_\theta = 192^3, 256^3$, and 384^3 and the clustering parameter $A_z = 3.0$ are sufficient for non-magnetic flows at $10^7 \leqslant Ra < 10^8$, $10^8 \leqslant Ra < 10^9$, and $Ra = 10^9$, respectively. Further refinement of the grid does not lead to significant changes. At the same time, the grid sensitivity study and the comparison between the maximum grid step in the bulk with the estimates of the Kolmogorov length scale indicate that the non-magnetic flow at $Ra = 10^9$ is somewhat under-resolved. This is viewed as acceptable because the focus of our work is on flows at high Hartmann numbers.

Suppression of velocity gradients by the magnetic field allows us to alleviate the resolution requirements for the radial and azimuthal directions. Our study shows that N_r and N_θ not higher than 192 and 256 grid points are needed to accurately resolve flow structures at $Ha \geqslant 450$ with $10^7 \leqslant Ra < 10^8$ and $10^8 \leqslant Ra \leqslant 10^9$, respectively. Considering the resolution along the axial coordinate, we need to take into account the Q2D character of the flow with weak axial gradients of velocity in the core (we must note that the gradients do not approach zero at high Ra even at the strongest magnetic fields) and thin Hartmann boundary layers at the top and bottom walls. This allows us to rely on grids with the smaller number of points, but stronger near-wall clustering. The grid sensitivity study shows that, depending on the value of Ha, N_z between 64 and 256 and A_z between 3 and 4 securing not less than 6 points within the Hartmann layer are sufficient.

As presented in detail in the supplementary material, our simulations show good grid convergence for Nu. The results for Re are less satisfactory, especially in flows with strong magnetic field effect. The structure and character of the time evolution of the flow allow us attribute this, at least partially, to the effect of strong and slow (on the time scale of many tens of convective units; see, e.g. figure 1(e)) fluctuations of velocity. Unfeasibly large averaging times are needed to eliminate this factor.

3. Results

3.1. *Spatial structure of the flow*

The flow structure for several typical cases is illustrated in figure 1. Flows without magnetic field (see figures 1a and 1b) are turbulent. The spatial structure in the horizontal cross-section (middle column) and the correlation between the velocity signals measured along a vertical line, indicate the presence of a large-scale circulation (LSC) with upward or downward flow zones.

The magnetic field drastically changes the flow. We observe suppression of small-scale velocity gradients and formation of large-scale anisotropic structures dominating the flow (see plots in the left and middle columns of figures 1(c)-(f)). This is associated with a reduction of amplitude and frequency of velocity fluctuations (see the plots in the right column of figures 1(c)-(f)) and, as we will discuss in section 3.2, an increase of Nu and Re. Similar flow transformations were detected in recent measurements of Zürner *et al.* (2020) and simulations of Liu *et al.* (2018); Yan *et al.* (2019) for lower Rayleigh numbers.

The strength of the magnetic field effect determining the degree of the flow transformation correlates with the ratio between Ra and Ra_c. At $Ra \gg Ra_c$ (see figures 1d and 1f), the large-scale velocity structures are anisotropic (elongated in the direction of the magnetic field) but succeptible to 3D instabilities and evolve on the background of 3D small-scale velocity fluctuations. At Ra larger, but not much larger than Ra_c (see figures 1c and 1e), the anisotropy is much stronger and 3D fluctuations are much weaker.

In the latter case, nearly Q2D upward and downward streams occupy the flow domain. Interestingly, these flows, in paricular the flow at $Ra/Ra_c \approx 5$ shown in figure 1e, are principally different from the other recently identified Q2D magnetoconvection regimes: the wall modes of Liu *et al.* (2018) and the cellular and columnar regimes found in an infinite horizontal layer by Yan *et al.* (2019). The former is not surprising, since the simulations of Liu *et al.* (2018) find the wall mode regimes at $Ra/Ra_c \sim 1$ or < 1, but not at higher Ra/Ra_c. For example, the wall modes were not found at $Ra/Ra_c = 4.05$.

The discrepancy with the results of Yan *et al.* (2019) obtained for an infinite horizontal layer appears more significant. Unlike the 'cells' reminiscent of the linear instability modes or the 'columns' found in their simulations, the dominant feature of the flow in figure 1e can be described as a system of ascending and descending planar jets often originating at the sidewall and extending into the bulk of the flow. We should mention that the horizontal velocity is strong in this flow ($\langle u_r^2 + u_\theta^2\rangle_{V,t}/\langle u_z^2\rangle_{V,t} \approx 0.44$ in comparison to ≈ 0.27 for the case in figure 1f). The regime is reminiscent of Q2D extended vortex sheets often found in MHD turbulent flows with strong magnetic field effect (see, e.g., Zikanov & Thess (1998)). The fact that this regime rather than the cellular or columnar regimes of Yan *et al.* (2019) is realized in our flow can be attributed to smaller Pr ($Pr = 1$ was used by Yan *et al.* (2019)) or, much more likely, the presence of sidewalls.

The wall mode regime is found in our simulations at $Ra/Ra_c \to 1$. As an illustration, figure 2 shows the instantaneous distributions of convective flux u_zT in flows with $Ra = 10^7$ (also used by Liu *et al.* (2018)) and several values of Ha. The structure of the wall modes is qualitatively similar to the structure observed by Liu *et al.* (2018) (see figure 2c). Significant flow and heat transfer are limited to tongue-like zones attached to the sidewall. There are noticeable differences, though. The entire wall-mode structure rotates clockwise or anticlockwise in our system. The effect of rotation is illustrated by the almost axisymmetric distribution of the time-averaged heat flux shown in figure 2d. Another difference is the transformation of wall modes at increasing Ra/Ra_c. As in the simulations of Liu *et al.* (2018), the wall modes extend further from the wall. The new feature that can be plausibly attributed to rotation is that the wall-mode zones curve (see figure 2b) and form Q2D vortices (see figure 2a). We leave a detailed analysis of properties and physical mechanisms of wall modes to future studies and only mention here that observed behaviour is qualitatively similar to that in RBC with rotation (Zhong *et al.* 1991; Ecke *et al.* 1992; Zhang *et al.* 2019).

3.2. *Global transport properties*

All computed values of Nu and Re are listed in the supplementary materials. They are also summarized and compared with the available experimental and numerical data in figure 3. The qualitative agreement between the numerical and experimental data is good. In particular, the increase of the slope of $Nu(Ra)$ and $Re(Ra)$ curves in flows with the magnetic field, which we discuss in detail below, is consistent between the simulations and the experiments. At the same time, the quantitative agreement is less convincing, with the computed values being consistently higher than in the experiments, especially in the experiment of Cioni *et al.* (2000). This situation is typical for thermal convection in low-Pr fluids and can be attributed to several known difficulties of the experimental procedure: (1) the ideal boundary conditions of constant temperature at the top and bottom plates cannot be accurately maintained; (2) temperatures at the top and bottom boundaries are not measured directly, which usually leads to a slight overestimation of the Rayleigh number; (3) complete avoidance of heat loses through the sidewall is impossible; (4) physical properties within a system are not constant, which results in inaccurate estimates of the Prandtl, Hartmann and Rayleigh numbers.

The estimates of the scaling behaviour of Nu and Re based on the data of our simulations are presented in table 1. Some of the respective lines are also shown in figure 3. The common regression method is applied to the computed time averaged values to determine the exponents β_{Nu} and β_{Re} and their standard errors, and the constants α_{Nu} and α_{Re} in the approximations $Nu \approx \alpha_{Nu} Ra^{\beta_{Nu}}$ and $Re \approx \alpha_{Re} Ra^{\beta_{Re}}$.

For flows with $Ha = 0$, some disagreement with the data of Cioni *et al.* (2000) is found (see figure 3a). At the same time, the computed value of β_{Nu} is in a good agreement with the value 0.29 ± 0.01 for $Pr = 0.025$ found in the experiments with the largest range $2 \times 10^5 \leqslant Ra \leqslant 8 \times 10^{10}$ by Glazier *et al.* (1999) performed at $\Gamma = 0.5, 1, 2$. The exponent β_{Re} is consistent with 0.46 ± 0.02 for $Pr = 0.025$ and 0.42 ± 0.03 for $Pr = 0.029$ found in measurements by Takeshita *et al.* (1996) and Zürner *et al.* (2019), respectively, and with 0.45 ± 0.04 for $Pr = 0.021$ in numerical simulations by Scheel & Schumacher (2017).

An imposed magnetic field reduces the rate of heat transfer and kinetic energy in the entire studied range of Ra. At the same time, growth of Nu and Re becomes faster. In particular, the slope β_{Nu} increases from 0.298 at $Ha = 0$ to about 0.574 at $Ha = 1400$. Similar increase is observed for β_{Re} (see table 1 and figure 3). The results are consistent with the data of (Cioni *et al.* 2000), the only experiment in the interesting for us range of Ra and Ha.

The Nusselt $\widetilde{Nu} = (Nu - 1)/(Nu_{Ha=0} - 1)$ and Reynolds $\widetilde{Re} = Re/Re_{Ha=0}$ numbers normalized by their reference values at $Ha = 0$ are shown in figure 4. The universal scaling behaviour of $\widetilde{Nu} = 1/(1 + \alpha_{\widetilde{Nu}}(Ha/Ha_c)^{\beta_{\widetilde{Nu}}})$ and $\widetilde{Re} = 1/(1 + \alpha_{\widetilde{Re}}(Ha/\sqrt{Ha_c})^{\beta_{\widetilde{Re}}})$ was proposed by Zürner *et al.* (2020). To verify this hypothesis, we plot $1/\widetilde{Nu} - 1$ and $1/\widetilde{Re} - 1$ vs $Ha/Ra^{1/2}$ in logarithmic scales. The computed data provide $\beta_{\widetilde{Nu}} = 1.305 \pm 0.049$ and $\beta_{\widetilde{Re}} = 0.549 \pm 0.034$.

The qualitative agreement between the simulations and the experiments, especially with the experiments by Cioni *et al.* (2000), is observed for $\widetilde{Nu}$ at $Ra > Ra_c$ ($Ha/Ra^{1/2} \sim 0.1$) and $Ra \gg Ra_c$ ($Ha/Ra^{1/2} < 0.1$) in figure 4a. The results indicate that universal power is approached for flows at high Rayleigh numbers. At the same time, the standard

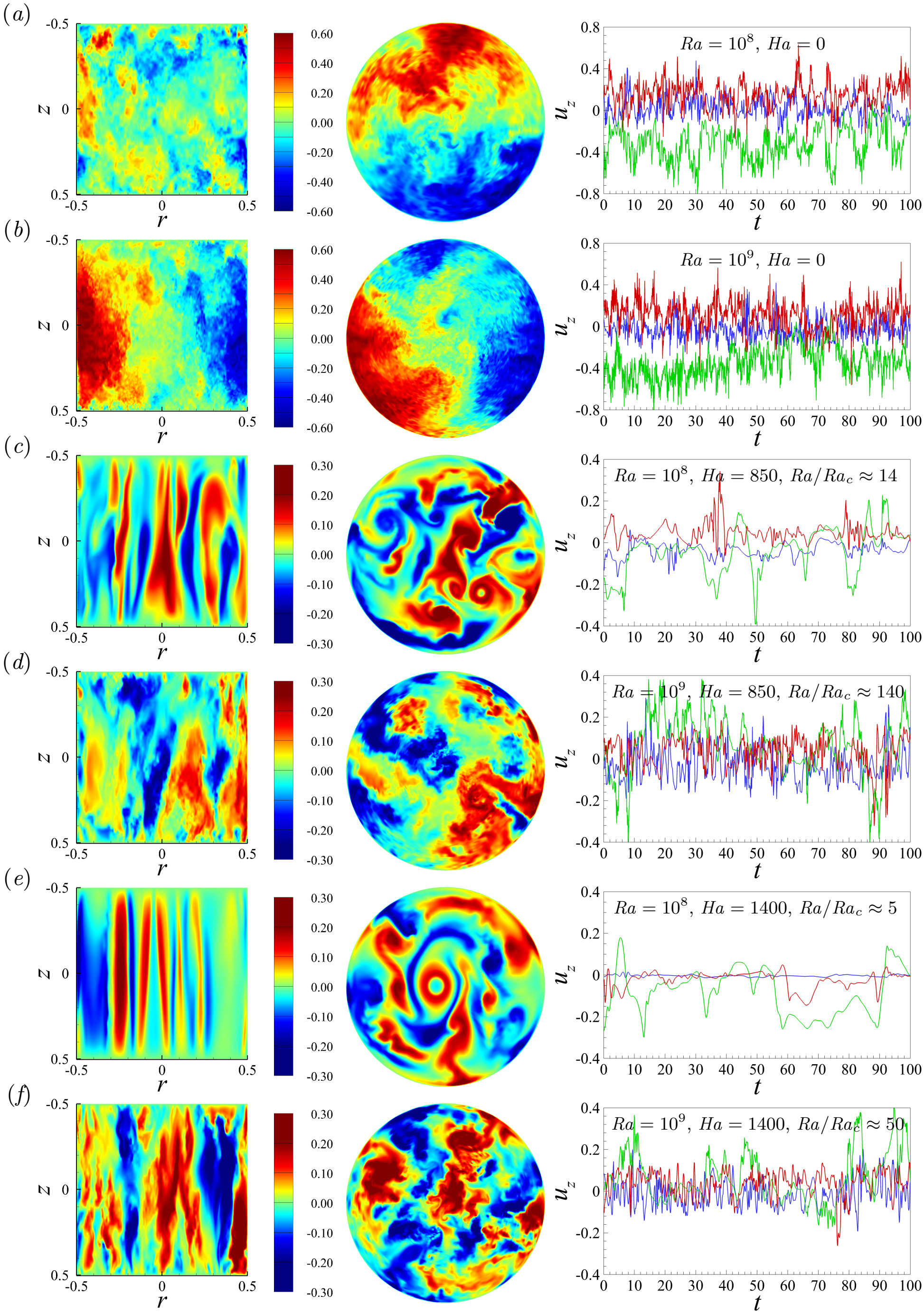

FIGURE 1. Snapshots of the vertical velocity in the vertical (left column) and horizontal mid-plane (center column) cross-sections, and time signals of u_z (right column) at $\theta = 0$, $z = 0.25$ (——), 0 (——), -0.25 (——), and $r = 0.42$ (e), 0.44 (a, c, d, f), 0.46 (b) are shown. The parameters (Ra, Ha and the ratio between Ra and Ra_c of the Chandrasekhar (1961) stability limit) are indicated in the right column.

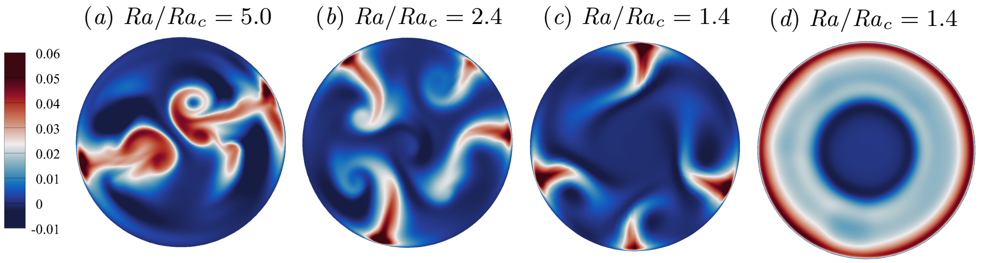

FIGURE 2. Snapshots of the convective flux u_zT in the horizontal mid-plane of the cylinder at $Ra = 10^7$: $Ra/Ra_c = 5.0$, $Ha = 450$ (a), $Ra/Ra_c = 2.4$, $Ha = 650$ (b), $Ra/Ra_c = 1.4$, $Ha = 850$ (c). Time averaged convective flux at $Ra = 10^7$ and $Ha = 850$ is shown in (d).

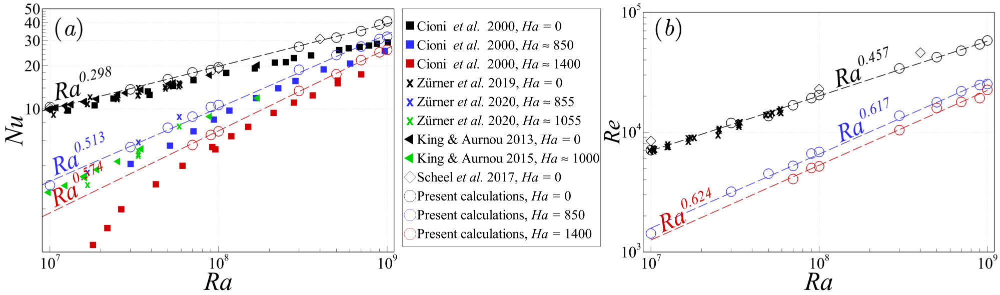

FIGURE 3. Nusselt number Nu vs Ra (a) and Reynolds number Re vs Ra (b) with and without magnetic field. Experimental and numerical data for $\Gamma = 1$ are shown for comparison. Slope lines $\backsim Ra^{\beta}$ are plotted for guidance.

Ra	Ha	α_{Nu}	β_{Nu}	α_{Re}	β_{Re}
$10^7 - 10^9$	0	0.0819	0.298 ± 0.005	4.427	0.457 ± 0.006
$10^7 - 10^9$	450	0.0064	0.420 ± 0.008	0.192	0.586 ± 0.010
$10^7 - 10^9$	650	0.0019	0.476 ± 0.007	0.139	0.591 ± 0.018
$10^7 - 10^9$	850	0.0008	0.513 ± 0.009	0.076	0.617 ± 0.012
$10^8 - 10^9$	1400	0.0002	0.574 ± 0.009	0.054	0.624 ± 0.033

TABLE 1. Scaling coefficients in the approximations $Nu \approx \alpha_{Nu} Ra^{\beta_{Nu}}$ and $Re \approx \alpha_{Re} Ra^{\beta_{Re}}$ based on the data of the present simulations (see figure 3).

error is higher and coefficient of determination (R^2) is lower than for the scaling $Nu \sim Ra^{\beta_{Nu}}$ presented above ($R^2 = 0.943$ in comparison to $R^2 = 0.998$ for $Nu \sim Ra^{\beta_{Nu}}$ at $Ha = 1400$). Similar situation is observed for the normalized Reynolds numbers in figure 4b.

We expect an increase of the exponents $\beta_{\widetilde{Nu}}$ and $\beta_{\widetilde{Re}}$ in the wall mode regime at $Ra \sim Ra_c$ ($Ha/Ra^{1/2} \sim 0.25$), however the measurements of Zürner *et al.* (2020) for $1/\widetilde{Re} - 1$ show higher slope line $\sim (Ha/Ha_c)^{1.73 \pm 0.05}$ for a wide range of Ra and Ha. The discrepancy with this result and the presence of even stronger deviations in experimental data for moderate Ra can be attributed to the limitations of the ultrasound Doppler velocimetry (UDV) used to probe the flow field discussed by Zürner *et al.* (2020).

The estimates of the thickness of the thermal boundary layer are presented in the supplementary materials. The common slope method used in the experiments (Takeshita

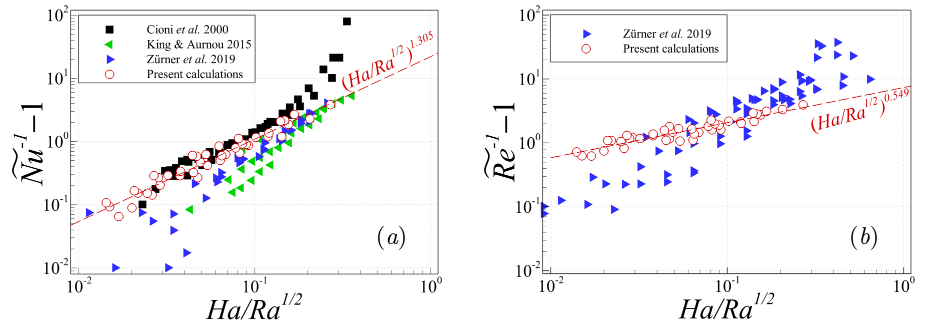

FIGURE 4. Normalized Nusselt number $\widetilde{Nu}$ vs $Ha/Ra^{1/2}$ (a) and Reynolds number $\widetilde{Re}$ vs $Ha/Ra^{1/2}$ (b). Experimental data $\Gamma = 1$ are shown for comparison. Slope lines $\backsim (Ha/Ra^{1/2})^{\beta}$ are plotted for guidance.

et al. 1996) and simulations (Liu *et al.* 2018) is applied, i.e. the intersection point of the tangent of the time-averaged mean temperature profile near the sidewall and the horizontal line drawn through the mean value is taken. We only mention here that the results of the present simulations deviate by not more than 2% from the theoretical value $\delta_T \approx 1/(2Nu)$ of Grossmann & Lohse (2001), even in the presence of magnetic field.

4. Concluding remarks

We have performed direct numerical simulations of Rayleigh-Bénard convection in a cylinder with imposed vertical magnetic field. The range of high Ra and Ha never previously explored in numerical simulations was considered. The computations were performed on large grids with adequate resolution of internal features and boundary layers.

The new regime in the form of nearly Q2D upward and downward planar jets originating at the sidewalls and extending into the flow domain is identified at Ra larger, but not much larger than Ra_c. The structures are reminiscent of Q2D extended vortex sheets found in MHD turbulence (see, e.g., Zikanov & Thess (1998)). Our results also show existence of rotating tongue-like wall modes at $Ra \to Ra_c$, in apparent qualitative similarity with rotating RBC (Ecke *et al.* 1992; Zhang *et al.* 2019).

The results of our DNS are consistent with available experimental and numerical data. In particular, we find faster growth of Nu and Re with Ra in flows with strong magnetic fields. This effect can only be plausibly attributed to the formation of coherent large-scale Q2D structures in the flow field (see section 3.1). The scaling laws for normalized Nusselt and Reynolds numbers reveal the same tendency as the experimental data, namely that the global transport properties approach a universal power law at $Ra \gg Ra_c$.

The presented work is considered by the authors as the beginning of a larger and more detailed study. Future investigations of the system are undoubtedly warranted. In particular, it would be interesting to further analyze the properties and physical mechanisms of the newly discovered Q2D regime, the behaviour of wall modes, the transport properties at $Ra > 10^9$ and $Ha > 1400$, and, finally, the apparent, albeit evidently incomplete, similarities between RBC with magnetic field and rotation.

Financial support is provided by the US NSF (Grant CBET 1803730) and the DFG grant KR 4445/2 − 1. Computer time is provided by the Computing Center of the Technische Universität Ilmenau and the Leibniz Rechenzentrum Garching within Large Scale project pr62se.

REFERENCES

Akhmedagaev, R., Zikanov, O., Krasnov, D. & Schumacher, J. 2020 Rayleigh-Bénard convection in strong vertical magnetic field: flow structure and verification of numerical method , arXiv: 2002.09404.

Aurnou, J. M. & Olson, P. L. 2001 Experiments on Rayleigh–Bénard convection, magnetoconvection and rotating magnetoconvection in liquid gallium. *J. Fluid Mech.* **430**, 283–307.

Burr, U. & Müller, U. 2001 Rayleigh–Bénard convection in liquid metal layers under the influence of a vertical magnetic field. *Phys. Fluids* **13** (11), 3247.

Busse, F. H. 2008 Asymptotic theory of wall-attached convection in a horizontal fluid layer with a vertical magnetic field. *Phys. Fluids* **20** (2), 024102.

Chandrasekhar, S. 1961 *Hydrodynamic and hydromagnetic stability*. Clarendon Press.

Cioni, S., Chaumat, S. & Sommeria, J. 2000 Effect of a vertical magnetic field on turbulent Rayleigh-Bénard convection. *Phys. Rev. Lett.* **62** (4).

Davidson, P. A. 2016 *Introduction to Magnetohydrodynamics*. Cambridge University Press.

Ecke, R., Zhong, F. & Knobloch, E. 1992 Hopf bifurcation with broken reflection symmetry in rotating Rayleigh-Bénard convection. *Europhys. Lett.* **19** (3), 177–182.

Gelfgat, A. Yu. & Zikanov, O. 2018 Computational modeling of magnetoconvection: effects of discretization method, grid refinement and grid stretching. *Comp. Fluids* **175**, 66–82.

Glazier, J. A., Segawa, T., Naert, A. & Sano, M. 1999 Evidence against 'ultrahard' thermal turbulence at very high Rayleigh numbers. *Nature* **398**, 307–310.

Grossmann, S. & Lohse, D. 2001 Thermal convection for large Prandtl numbers. *Phys. Rev. Lett.* **86**, 3316.

Houchens, B. C., Witkowski, L. M. & Walker, J. S. 2002 Rayleigh–Bénard instability in a vertical cylinder with a vertical magnetic field. *J. Fluid Mech.* **469**, 189–207.

King, E. M. & Aurnou, J. M. 2015 Magnetostrophic balance as the optimal state for turbulent magnetoconvection. *Proc. Natl. Acad. Sci. USA* **112** (4), 990–994.

Krasnov, D., Zikanov, O. & Boeck, T. 2011 Comparative study of finite difference approaches to simulation of magnetohydrodynamic turbulence at low magnetic Reynolds number. *Comp. Fluids* **50**, 46–59.

Krasnov, D., Zikanov, O. & Boeck, T. 2012 Numerical study of magnetohydrodynamic duct flow at high Reynolds and Hartmann numbers. *J. Fluid Mech.* **704**, 421–446.

Lim, Z. L., Chong, K. L., Ding, G. & Xia, K. 2019 Quasistatic magnetoconvection: heat transport enhancement and boundary layer crossing. *J. Fluid Mech.* **870**, 519–542.

Liu, W., Krasnov, D. & Schumacher, J. 2018 Wall modes in magnetoconvection at high Hartmann numbers. *J. Fluid Mech.* **849**, R2.

Nakagawa, Y. 1957 Experiments on the inhibition of thermal convection by a magnetic field. *Proc. R. Soc. London* **240** (1220), 108–113.

Ni, M.-J., Munipalli, R., Huang, P., Morley, N. B. & Abdou, M. A. 2007 A current density conservative scheme for incompressible MHD flows at a low magnetic Reynolds number. Part I: On a rectangular collocated grid system. *J. Comp. Phys.* **227**, 174–204.

Ozoe, H. 2005 *Magnetic Convection*. Imperial College Press.

Scheel, J. D. & Schumacher, J. 2017 Predicting transition ranges to fully turbulent viscous boundary layers in low Prandtl number convection flows. *Phys. Rev. Fluids* **2** (12), 123501.

Takeshita, T., Segawa, T., Glazier, J. A. & Sano, M. 1996 Thermal Turbulence in Mercury. *Phys. Rev. Lett.* **76** (9), 1465–1468.

Weiss, N. O. & Proctor, M. R. E. 2014 *Magnetoconvection*. Cambridge University Press.

Yan, M., Calkins, M. A., Maffei, S., Julien, K., Tobias, S. M. & Marti, P. 2019 Heat transfer and flow regimes in quasi-static magnetoconvection with a vertical magnetic field. *J. Fluid Mech.* **877**, 1186–1206.

Zhang, X., van Gils, D. P. M., Horn, S., Wedi, M., Zwirner, L., Ahlers, G., Ecke, R. E., Weiss, S., Bodenschatz, E. & Shishkina, O. 2019 Boundary zonal flow in rotating turbulent Rayleigh-Bénard convection , arXiv: 1911.09584.

Zhao, Y. & Zikanov, O. 2012 Instabilities and turbulence in magnetohydrodynamic flow in a toroidal duct prior to transition in Hartmann layers. *J. Fluid Mech.* **692**, 288–316.

Zhong, F., Ecke, R. & Steinberg, V. 1991 Asymmetric modes and the transition to vortex structures in rotating Rayleigh-Bénard convection. *Phys. Rev. Lett.* **67** (18), 2473.

Zikanov, O., Listratov, Ya. & Sviridov, V. G. 2013 Natural convection in horizontal pipe flow with strong transverse magnetic field. *J. Fluid Mech.* **720**, 486–516.

Zikanov, O. & Thess, A. 1998 Direct numerical simulation of forced MHD turbulence at low magnetic Reynolds number. *J. Fluid Mech.* **358**, 299–333.

Zürner, T., Schindler, F., Vogt, T., Eckert, S. & Schumacher, J. 2019 Combined measurement of velocity and temperature in liquid metal convection. *J. Fluid Mech.* **876**, 1108–1128.

Zürner, T., Schindler, F., Vogt, T., Eckert, S. & Schumacher, J. 2020 Flow regimes of Rayleigh-Bénard convection in a vertical magnetic field , arXiv: 2002.07414.